AIP | Journal of Applied Physics

Environment-dependent surface structures and stabilities of SnO2 from the first principles

Canhui Xu, Yong Jiang, Danqing Yi, Shunping Sun, and Zhiming Yu

Citation: J. Appl. Phys. **111**, 063504 (2012); doi: 10.1063/1.3694033

View online: http://dx.doi.org/10.1063/1.3694033

View Table of Contents: http://jap.aip.org/resource/1/JAPIAU/v111/i6

Published by the American Institute of Physics.

Related Articles

Additional information on J. Appl. Phys.

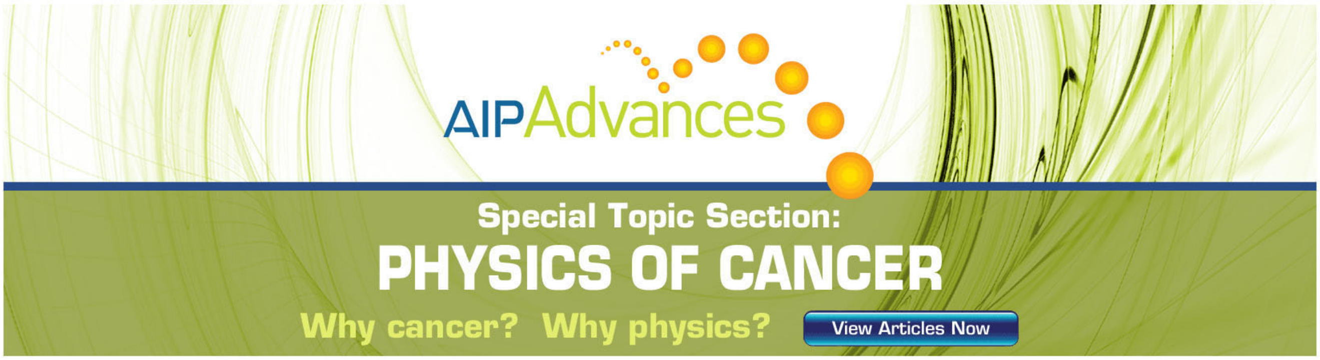

JOURNAL OF APPLIED PHYSICS **111**, 063504 (2012)

Environment-dependent surface structures and stabilities of SnO_2 from the first principles

Canhui Xu, Yong Jiang,[a] Danqing Yi,[a] Shunping Sun, and Zhiming Yu
School of Materials Science and Engineering, Central South University, Changsha 410083, People's Republic of China and Key Lab of Nonferrous Materials, Ministry of Education, Central South University, Changsha, Hunan 410083, People's Republic of China

(Received 30 September 2011; accepted 18 February 2012; published online 19 March 2012)

We have employed density functional theory to investigate the (110), (101), (100), and (001) surfaces of SnO_2 within the pseudopotential, plane-wave method. Based on a thermodynamic defect model, the surface stabilities were evaluated as functions of oxygen partial pressure and temperature. Calculations showed that, below 600 K, the stoichiometric (110) has the lowest surface energy for a wide range of oxygen partial pressures, followed by the (100), (101), and (001). At higher temperatures, the stability transition from the stoichiometric to a Sn-rich termination tends to occur on all these surfaces (except the (001)) at ultrahigh vacuum. Such transitions may shift to higher pressures with increasing temperature. An equilibrium surface phase diagram was then developed to illustrate the environment dependence of these surfaces. The electronic structure of the stoichiometric (110) was also analyzed based on the electron density of states and differential charge density distribution. © *2012 American Institute of Physics*. [http://dx.doi.org/10.1063/1.3694033]

I. INTRODUCTION

Tin dioxide (SnO_2) is a well-known, wide band-gap (~ 3.6 eV) semiconductor with an interesting combination of low electrical resistance and high optical transparency and has been widely used in applications, such as solar cells, flat panel displays, touch controls, and defrosting windows.[1–3] Especially, oxygen chemistry of SnO_2 surfaces sensitively relies on the ambient environmental atmosphere, which is reflected by the measurable change of electrical conductivity,[4] making it also attractive for some new applications, including oxidation catalysts and gas sensors.[5] More recently, nanofabricated SnO_2 was suggested as a promising alternative to the conventional anode materials in lithium-ion batteries,[6] due to its high capacity as well as the low active voltage, where the anode performance is largely affected by the surface quality of SnO_2 nanoparticles. For its unique properties, SnO_2 surfaces attracted a large amount of research efforts with both theoretical and experimental approaches.

Low-index SnO_2 surfaces with ideal bulk terminations have been first investigated using first-principle methods.[7,8] These calculations concluded that the (110) surface is the most stable one, followed by (100), (101), and (001). The oxygen sensitivity of SnO_2 surfaces is virtually due to the variable valence of Sn atoms, which allows this material to actively react with adsorbed oxygen from the ambient. Detailed surface structures of SnO_2 are determined by the chemical potentials of the participating species, which in turn are determined by environmental conditions, such as temperature and oxygen partial pressure (the later represents the oxygen content of the ambient atmosphere). The temperature dependence of surface oxygen coverage, as well as its transient behaviors at various temperatures, was initially investigated by kinetic Monte Carlo simulations by Pulkkinen *et al.*[9] It was suggested that the ionic adsorbate transition from O_2^- to O^- dominance on surface occurs at about 700 K, where the effects of oxygen partial pressure on the coverage of physisorbed oxygen are trivial. Batzill *et al.*[10] further investigated the temperature dependence of surface transitions from stoichiometric to reduced terminations and found that such a transition initiates at 440 ~ 520 K, 610 ~ 660 K, or 560 ~ 660 K for the (110), (100), or (101) surface, respectively. The oxidation states of surfaces, as well as the dependence of surface stabilities on oxygen chemical potential, have been also evaluated using density functional theory (DFT) calculations by the same research group. Very recently, Ágoston *et al.*[11] calculated the thermodynamic equilibrium diagram of the (110) surface that clearly reveals how the termination changes from stoichiometric to reduced (or vice versa) with oxygen chemical potential changes. However, oxygen chemical potential itself is an environment-dependent quantity, i.e., it is a function of the two major environmental factors: temperature, T, and oxygen partial pressure, P_{O2}. Up to now, no definite models have been proposed and used to clarify how each individual factor, as well as their interplay, affects the surface structures (and hence the surface properties) of SnO_2.

A stable oxide surface that can be regarded as the end result of the dynamic balance of surface oxygen adsorption and desorption processes must be modeled, as in a thermal equilibrium at a certain temperature with an atmosphere containing a certain oxygen concentration. In this work, from the concepts of first-principles thermodynamics, we expressed the surface energy of SnO_2 as a direct function of temperature and oxygen partial pressure and extended our DFT investigations

---

[a] Authors to whom correspondence should be addressed. Tel.: +86-731-88836320. Fax: +86-731-88830263. Electronic addresses: yjiang@csu.edu.cn and yioffice@csu.edu.cn.

to all non-stoichiometric (both Sn- and O-terminated) surfaces of (110), (101), and (100). This approach enabled us to predict and compare surface stabilities of SnO_2 under more practical conditions, i.e., for any given T and P_{O2}. Moreover, the electronic structure of the stoichiometric (110), as the most stable surface at the low to medium temperature range (below 600 K), has been exemplarily investigated to understand the chemical reactivity of the surface.

II. COMPUTATIONAL METHODS AND ATOMIC MODELS OF SURFACES

All density functional theory calculations were performed on periodic solids using the Vienna *ab initio* simulation package (VASP)[12] based on the plane-wave basis set. The electron-core interaction was described by the projector augmented wave method (PAW)[13] within the frozen-core approximation. The plane-wave basis sets were generated with valence configurations of Sn-$4d^{10}5s^{2}5p^{2}$ and O-$2s^{2}2p^{4}$. To sample the Brillouin zone, the k-meshes generated automatically according to the Monkhorst–Pack method.[14] The electronic minimization algorithm for static total energy calculations was based on a residual minimization scheme—direct inversion in the iterative subspace (RMM-DIIS). Ground-state atomic geometries of surfaces were optimized by minimizing the Hellman-Feyman forces using a combined blocked Davidson + RMM-DIIS algorithm until the total forces on each ion were converged to 0.02 eV/Å. The optimal choice of exchange-correlation (XC) functional was based on the comparison of predicted bulk properties with their experimental counterparts. The XC functionals tested included local-density approximation (LDA), the generalized gradient approximation (GGA) with Perdew-Wang-91 functional (PW91),[15] and the Perdew-Burke-Ernzerhof (PBE) functional.[16]

The crystalline structure of SnO_2 is rutile (tetragonal) at room temperature and normal pressure and belongs to spacegroup D_{4h}^{14} ($P4_2/mnm$). In the six-atom primitive cell, each tin atom is six-coordinated in a slightly distorted oxygen octahedron, as presented in Fig. 1. The atoms are located as follows: O at $\pm(u, u, 0; u+\frac{1}{2}, \frac{1}{2}-u, \frac{1}{2})$ and Sn at $(0, 0, 0; \frac{1}{2}, \frac{1}{2}, \frac{1}{2})$ in units (a, a, c). The lattice constants were experimentally measured as $a = 4.7374$ and $c = 3.1864$ Å with the internal parameter of $u = 0.306$.[17] Before calculating the surfaces, we first evaluated various XC functionals by predicting experimental lattice properties of SnO_2 through fitting the energy-volume data to the Murnaghan's equation of state.[18] The calculations were implemented on a primitive unit cell with a 9 × 9 × 15 Monkhorst-Pack k-point grid. The plane-wave cutoff energy of 400 eV was used throughout this work and was regarded high enough for calculating SnO_2 surfaces.[19] Due to the variable valence of Sn, this material may readily lose oxygen atoms at its surface, and hence, the oxygen chemistry at the surface is sensitive to the ambient environment conditions. Through exchanging oxygen with the ambient atmosphere, different oxidation degrees of a SnO_2 surface could result: oxidized (stoichiometric), reduced (Sn-terminated), and over-adsorbed (O-terminated).[20] It is of realistic significance to investigate all possible surface terminations. Low-index surfaces of (110), (100), (101), and (001) are more interesting to us in the present study. Following the classification by Sayle *et al.*,[21] the (001) can be described as Type I surfaces: they are stacks of charge neutral planes, with each plane retaining the SnO_2 stoichiometry, and therefore do not have nonstoichiometric counterparts. All other stoichiometric surfaces of interest, i.e., (100), (101), and (110), belong to Type II surfaces, which consist of neutral repeatable (O-Sn-O or O-SnSnOO-O) sandwiches and, hence, have zero perpendicular dipole moment to surface. Their nonstoichiometric counterparts, i.e., the O- or Sn-terminated (100), (101), and (110) surfaces, have non-zero, but equal and opposite normal dipole moments on both sides of the slabs, which would exactly cancel out each other across the vacuum. Therefore, all these surfaces could be calculated in their periodic slabs without the necessity of dipole corrections. Figure 2 shows the atomic models of all the surfaces mentioned above, each with its smallest possible unit cells in x- and y-dimensions. The number of layers for each surface was optimally determined by a series of full relaxation calculations, varying the slab thickness until the surface energy was converged. The numbers of repeatable construction blocks and the corresponding supercell sizes of the surface slabs are provided in Table I.

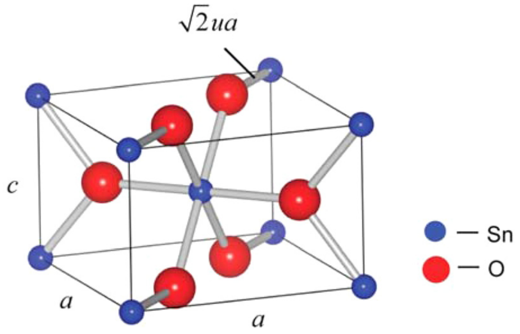

FIG. 1. (Color online) Primitive tetragonal unit cell of SnO_2.

III. RESULTS AND DISCUSSIONS

A. Bulk properties

The results of DFT bulk structure optimization using various exchange correlation functionals are summarized in Table II and compared with previous calculations and experiments.[8,20,22–25] It is found that PAW-GGA (PW91) and PAW-PBE predict quite similar results for lattice structures and bulk modulus, which is expectable in that the PBE functional differs from the PW91 only by using a simplified exchange enhancement factor. Both types of GGA overestimate the experimental values by ~1.8%. The overestimation resulting from the gradient corrections has an effect of isotropic (negative) pressure on the crystal, so that the c/a ratio and the u parameter remain almost unchanged to experiment (0.673 and 0.306, respectively). Our PAW-LDA prediction has a much improved accuracy on bulk properties compared to the GGAs' and other previous theoretical results: the lattice parameters calculated by PAW-LDA (a = 4.731 Å, c = 3.197 Å, and u = 0.306) are in almost perfect agreement with the experimental data (a = 4.737 Å, c = 3.186 Å, and u = 0.306)[24,25] within

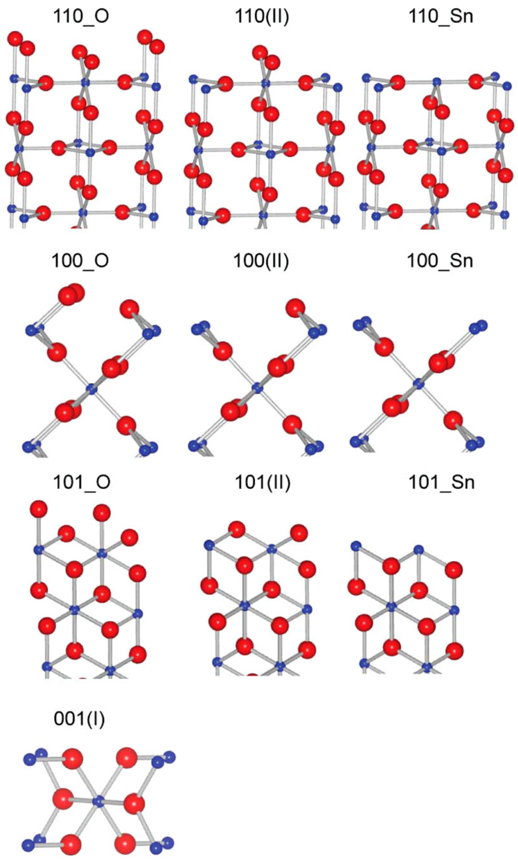

FIG. 2. (Color online) Atomic models of SnO_2 surfaces with different terminations as ideally cleaved from the bulk (red circles: O2–, blue circles: Sn4+). The surface types shown in the brackets follow the definition in Ref. 21.

an error of only ~0.5%. The bulk modulus predicted by PAW-LDA also agrees well within only a 3.7% error.

B. Surface energy

Surface stability is evaluated by surface energy, γ, which is often defined as[26]

$$\gamma = \frac{1}{2A}(E_{tot,surf} - E_{tot,bulk} + P\Delta V - T\Delta S), \qquad (1)$$

where A is the surface area defined in the slab, $E_{tot,surf}$ is the total energy of a surface slab, and $E_{tot,bulk}$ is the total energy of the counterpart bulk, which consists of the same number of atoms. ΔV is the volume change due to surface relaxation, which is normally small and can be ignorable. ΔS is mainly the vibrational entropy change due to the surface creation from a perfect crystal. The $-T\Delta S$ term tends to lower the surface free energy as T increases, but the resulted changes in the relative ordering of surface energies (stabilities) are often negligible (we will come back to this point at the end of this session). In practice, to predict a surface stability, the last two terms in Eq. (1) can be disregarded and only the contributions from the two total energies will be calculated. Such thermodynamic defect models and the corresponding approximations have been successfully applied to assess the stabilities of point defects in bulk oxides[27–29] and also other oxide surfaces.[10,26,30]

TABLE I. Atomic compositions of SnO_2 surface models.

Surface	Numbers of repeatable building blocks and supercell size	Compositions of slabs
	7 × [O-SnSnOO-O]	
(110)	3.19 × 6.69 × 35 Å	$Sn_{14}O_{26}$(–Sn), $Sn_{14}O_{28}$, $Sn_{14}O_{30}$(–O)
	13 × [O-Sn-O]	
(100)	4.73 × 3.20 × 43 Å	$Sn_{13}O_{24}$(–Sn), $Sn_{13}O_{26}$, $Sn_{13}O_{28}$(–O)
	8 × [OO-SnSn-OO]	
(101)	5.71 × 4.73 × 33 Å	$Sn_{16}O_{28}$(–Sn), $Sn_{16}O_{32}$, $Sn_{16}O_{36}$(–O)
	13 × [O-Sn-O]	
(001)	4.73 × 4.73 × 32 Å	$Sn_{13}O_{26}$

TABLE II. Calculated lattice parameters and bulk modulus in comparison with experiments and other calculations.

Methods	*a*, Å	*c*, Å	*c*/*a*	*u*	Bulk modulus, GPa
PAW-GGA(PW91)	4.819	3.242	0.673	0.306	181.8
PAW-PBE	4.823	3.243	0.672	0.306	180.4
PAW-LDA	4.731	3.197	0.676	0.306	209.9
US-GGA [Ref. 8]	4.778	3.232	0.676	0.306	
B3LYP [Ref. 20]	4.718	3.187	0.675	0.307	
LDA [Ref. 22]	4.74	3.128	0.66	0.307	218
GGA [Ref. 23]	4.82	3.29	0.683		
Experiment [Ref. 24,25]	4.737	3.186	0.673	0.306	218

As we have mentioned above, the detailed structure and property of an oxide surface are determined by its interaction with adsorbed oxygens. There have been a number of experimental and theoretical investigations that seek to uncover the mechanisms of SnO_2 surface reaction with oxygens, but most concentrated on the stoichiometric and reduced SnO_2 (110) and (101).[10,20,31–36] In this work, we focus on a series of low-index SnO_2 surfaces with all possible ideal terminations, either stoichiometric, reduced, or oxidized, under thermodynamic equilibrium with the ambient atmosphere and consider the surface oxidation as a two-step process,

$$Sn_{surf} + O_2^{ad} \overset{T,P}{\leftrightarrow} Sn_{surf} + 2[O] \overset{T,P}{\leftrightarrow} SnO_{2,surf}. \qquad (2)$$

Under certain T and P_{O2}, adsorbed oxygen molecules, O_2^{ad}, get dissolved into the surface, and then the dissolved oxygen, [O], combines with tin to gradually form tin oxide. When surface reactions reach thermodynamic equilibrium, i.e., $\Delta G = 0$ for oxide formation or decomposition, the sum of the elemental chemical potentials must be equal to the chemical potential of a crystalline SnO_2 as

$$\mu_{Sn,surf} + \mu_{O2}^{ad} = \mu_{Sn,surf} + 2\mu_{[O]} = \mu_{SnO2,surf} = \mu_{SnO2,bulk}. \qquad (3)$$

Thus, the surface energy of SnO_2 under thermodynamic equilibrium, γ, can be rewritten as

$$\begin{aligned}\gamma &= \frac{1}{2A}(E_{tot,surf} - N_{Sn}\mu_{Sn} - N_O\mu_O)\\ &= \frac{1}{2A}\left[E_{tot,surf} - N_{Sn}\mu_{SnO2,bulk} + (N_{Sn} - \frac{N_O}{2})\mu_{O2,gas}\right], \quad (4)\end{aligned}$$

where μ_i is the elemental chemical potential and N_i is the number of the corresponding atoms in the surface supercell. For a stoichiometric SnO_2 surface ($N_O = 2N_{Sn}$), the surface energy must be independent of μ_{O2}, while for a nonstoichiometric or defective surface ($N_O \neq 2N_{Sn}$), the surface energy becomes a linear function of μ_{O2} with a positive slope for the oxygen-deficient case or, vice versa, a negative slope for the oxygen-enriched case. Assuming oxygen in the ambient as an ideal gas, one can express the oxygen chemical potential μ_{O2} as a function of the ambient environmental conditions (T and P_{O2}) as[26]

$$\mu_{O2}(T,P) = \mu_{O2}^o(T) + kT\ln\left(\frac{p_{O2}}{p_{O2}^o}\right), \quad (5a)$$

$$\mu_{O2}(T,P) = [\mu_{O2}^o(0K) + \Delta H_{O2}(T) - T\Delta S_{O2}(T)] + kT\ln p_{O2}, \quad (5b)$$

where p_{O2}^o is taken to be 1 atm and k is the gas constant = 8.314 $J{\cdot}K^{-1}{\cdot}mol^{-1}$. Finally, the surface energy, γ, can be expressed as the function of temperature, T, and oxygen partial pressure, P_{O2}, as

$$\gamma = \frac{1}{2A}\left\{\begin{array}{l} E_{tot,surf} - N_{Sn}\mu_{SnO2,bulk} \\ +(N_{Sn} - \frac{N_O}{2})[\mu_{O2}^o(0K) + \Delta H_{O2}(T) - T\Delta S_{O2}(T) + kT\ln p_{O2}] \end{array}\right\}. \quad (6)$$

The temperature dependence of $E_{tot,surf}$ and μ_{SnO_2} would essentially cancel out each other in computing the surface energy and, thus, can be approximated by DFT calculations at 0 K. The major contribution for the temperature dependence of the surface energy comes from the energetic terms of O_2, among which $\Delta H_{O2}(T)$ and $\Delta S_{O2}(T)$ can be referred to experimentally measured values, as tabulated in JANAF tables[37] and redrawn in Fig. 3.

Table III summarizes our calculations of the low-index stoichiometric surfaces in comparison with other earlier theoretical results.[8,10,33,34,38,39] The surface energies calculated by different researchers using various GGA-type functionals are found to be very similar. The LDA predictions are 30% ~ 60% higher than the GGAs. The only full-potential PBE calculation performed by Batzill *et al.*[10] yields surface energies that lie about halfway between the LDA- and GGA-type pseudopotential results. Nevertheless, no matter what exchange-correlation functional was used, the same ordering of stability was confirmed by DFT: the most stable surface of SnO_2 is the (110) surface, followed by the (100), (101), and (001). If using the FP-PBE results as a reference (whenever experiments are unavailable), our PAW-GGA or PBE underestimates surface energy, while PAW-LDA does the opposite. Hence, we are able to predict the surface energies of SnO_2 with possible error ranges as $\gamma(110) \approx 1.19 \pm 0.19$, $\gamma(100) \approx 1.31 \pm 0.24$, $\gamma(101) \approx 1.61 \pm 0.19$, and $\gamma(001) \approx 2.03 \pm 0.20$ J/m^2. Evidently, the (101) has a surface energy much higher than that of the (110) and (100) and thus is expected to be less stable. The empirical shell model[39] predicted the surface energies that were closer to the LDA's than the GGA's, except only for the (101), which resulted in a reversed ordering between the (100) and the (101). Some experimental studies have also reported that the SnO_2 (101) can be made more stable than the (100) under some certain conditions,[40] which, however, should not be interpreted as a success of the shell model. Indeed, the prediction precision of the shell model calculation is rather limited and not comparable to that of DFT. The unusual stability of the (101) occasionally observed in these experiments encourages us to explore these surfaces for their dependence on ambient conditions.

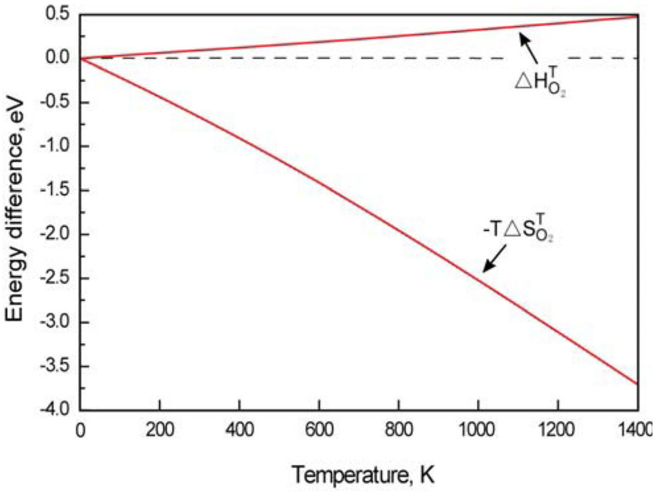

FIG. 3. (Color online) Experimentally measured energy differences, $\Delta H_{O2}(T)$ and $\Delta S_{O2}(T)$, as tabulated in JANAF tables Ref. 33.

According to Eq. (6), the surface energy of a nonstoichiometric surface can no longer be a constant value, but depends on the ambient conditions, i.e., T and P_{O2}. Figure 4 plots and compares the calculated surface energies of the low-index, non-stoichiometric surfaces as functions of P_{O2} at different temperatures. The upper limit of P_{O2} can be determined by requiring no net loss of oxygen from the surface under the thermodynamic equilibrium conditions, i.e., $\mu_{O2}^{ad} \leq \mu_{O2,gas}^O$ or $\ln p_{O2} \leq \ln p_{O2}^0 = 0$ (according to Eq. (5a)). It is clear from the graph that the O-terminated surface energies tend to increase with temperatures, but decrease with oxygen partial pressures, while the Sn-terminated surface energies exhibit the opposite tendency. At low temperatures (at or near room temperature), the stoichiometric termination of each surface yields the lowest surface energy over all the

TABLE III. Calculated surface energies of some stoichiometric surfaces (in units of J/m^2).

	Surface index			
Methods	110	100	101	001
PAW-LDA	1.38	1.55	1.79	2.23
PAW-GGA	1.06	1.14	1.47	1.88
PAW-PBE	1.00	1.07	1.42	1.83
US-LDA [Ref. 38]	1.66			
LDA [Ref. 34]	1.50			
US-GGA [Ref. 8]	1.04	1.14	1.33	1.72
PAW-GGA [Ref. 33]	1.01		1.44	
Shell model [Ref. 39]	1.38, 1.40	1.66, 1.65	1.55, 1.55	2.36, 2.37
FP-PBE [Ref. 10]	1.21	1.29	1.60	

range of pressures up to 1 atm, while its non-stoichiometric counterpart, either the O- or the Sn-terminated surface, always has a higher surface energy (and hence is less stable). With increasing temperature, the surface energies of the O-terminated surfaces further increase to even higher values, while those of the Sn-terminated surfaces decrease rapidly. Eventually, a surface transition from a stoichiometric to a Sn-rich termination may take place at ultrahigh vacuum (UHV): for instance, at 600 K, the Sn-terminated (101) surface (i.e., the (101)_Sn) becomes more stable than the stoichiometric (101) at $\ln P_{O2} \leq -65$. As one can expect, when temperature further increases, this transition point moves to higher (more practical) pressures: as shown in Fig. 4, at T = 1200 K, the transition start to occur at $\ln P_{O2} = \sim -17$ (or $P_{O2} = \sim 10^{-8}$ atm). One should notice that we have only considered surfaces with ideal terminations.

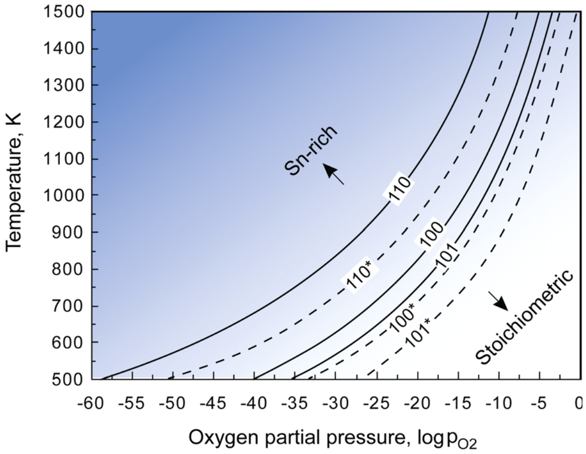

FIG. 5. (Color online) The calculated equilibrium surface phase diagram illustrates the environment dependence of SnO$_2$ surfaces. The solid curves are predicted by PAW-PBE and the dashed curves by PAW-LDA.

In reality, such a termination transition is made possible by a gradual and continuous loss of outermost layer oxygen atoms. Surface reconstruction might also form on a strongly reduced SnO$_2$ surface, as already observed in experiments:[5,10] at relatively low oxygen pressures, the (100) or (101) surface reconstruction may take place after losing all bridging oxygen atoms from its original stoichiometric termination, while on the (110) surface, the reconstruction

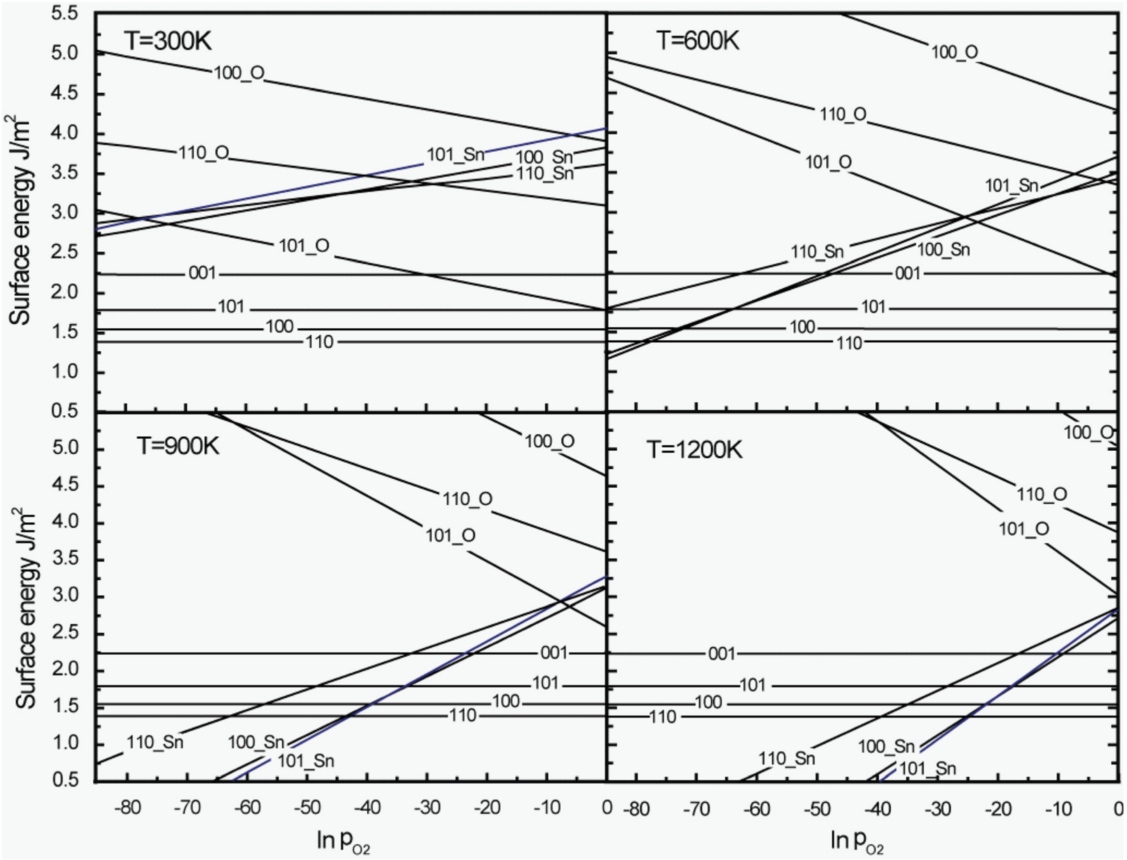

FIG. 4. (Color online) Calculated surface energies of various SnO$_2$ surfaces as a function of oxygen partial pressure at different temperatures.

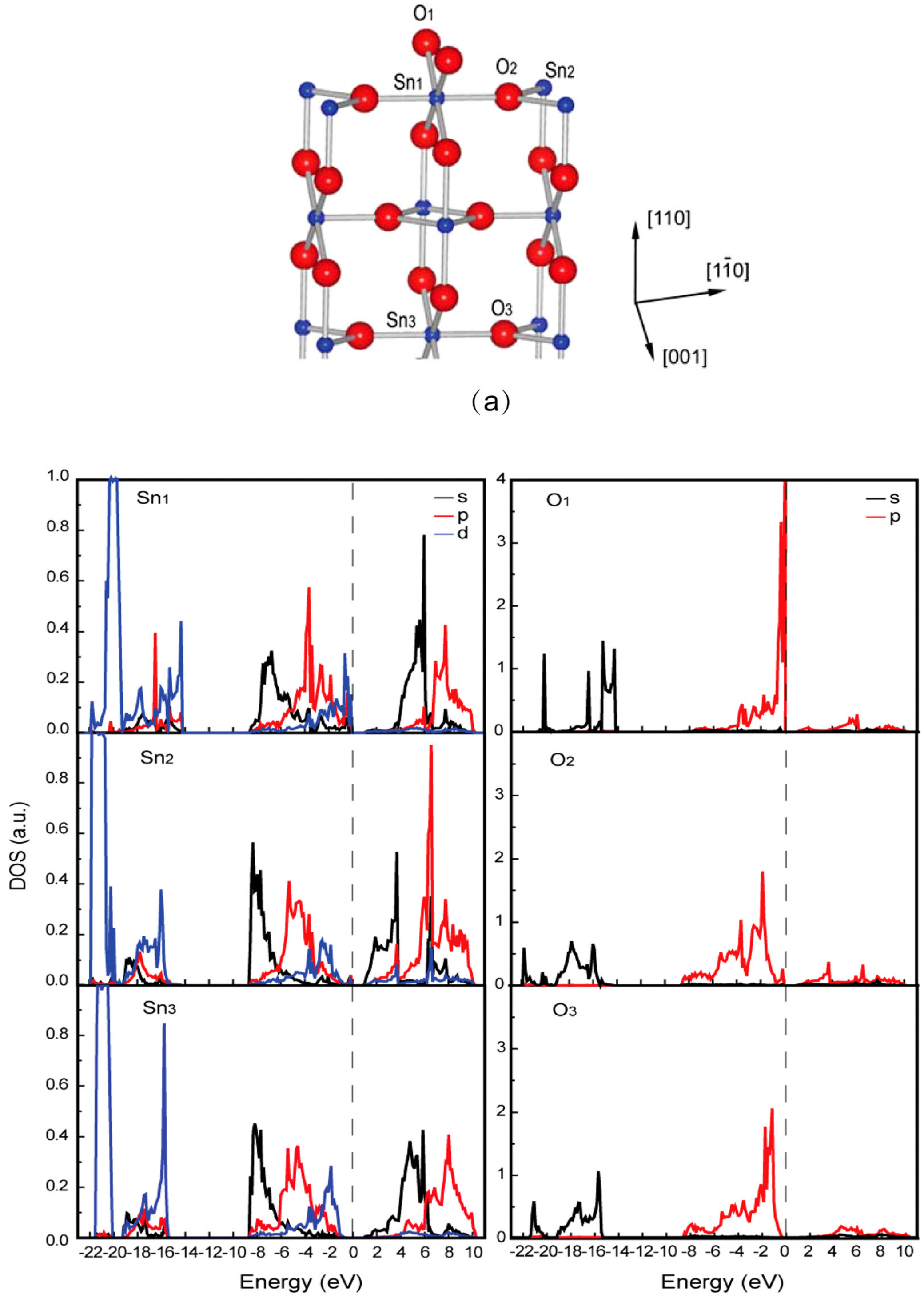

(a)

(b)

FIG. 6. (Color online) (a) The atomic structure and (b) valence electron density of states (DOS) of the stoichiometric (110) surface.

results from the complete loss of both bridging and in-plane oxygen atoms. Very recently, Ágoston *et al.*[11] investigated the reduction and reconstructions of the SnO_2 (110) surface using DFT, based on which they proposed an equilibrium surface phase diagram of the (110). Surface reconstruction would greatly affect surface reactivity and properties, but to reach such an equilibrium structure is not always feasible in many practical environments, where surface vacancies may form gradually and continuously and stabilize the surfaces. As a consequence, a more gradual transition from a stoichiometric to a Sn-rich termination would often result upon the exposure to reducing gaseous environments. Indeed, the continuous depletion of surface oxygen atoms has been observed at high temperature under the ultrahigh vacuum (UHV) condition for a series of initially fully oxidized SnO_2 surfaces using temperature-programmed, low energy, ion-scattering (TP-LEIS) techniques.[10] Using the results calculated by Eq. (6), we replot the environment dependence of SnO_2 surfaces in Fig. 5, which can be seen as the equilibrium surface phase diagram of SnO_2 without considering surface reconstructions. Each curve represents a "phase boundary" between the Sn-rich and the stoichiometric termination for a certain surface calculated by PAW-PBE (solid) or PAW-LDA (dashes): the area below the curve favors the formation of the stoichiometric termination, whereas the area above the curve favors the formation of the Sn-terminated surface. The actual "phase boundary" might very possibly lie between PAW-PBE and PAW-LDA predictions; hence, the region between the solid curve and its dashed counterpart defines the environment conditions in favor of intermediate terminations as the result of a gradual and continuous loss of surface oxygens. As predicted and shown in Fig. 4, an oxygen-rich termination can never be expectable for SnO_2 under any practical

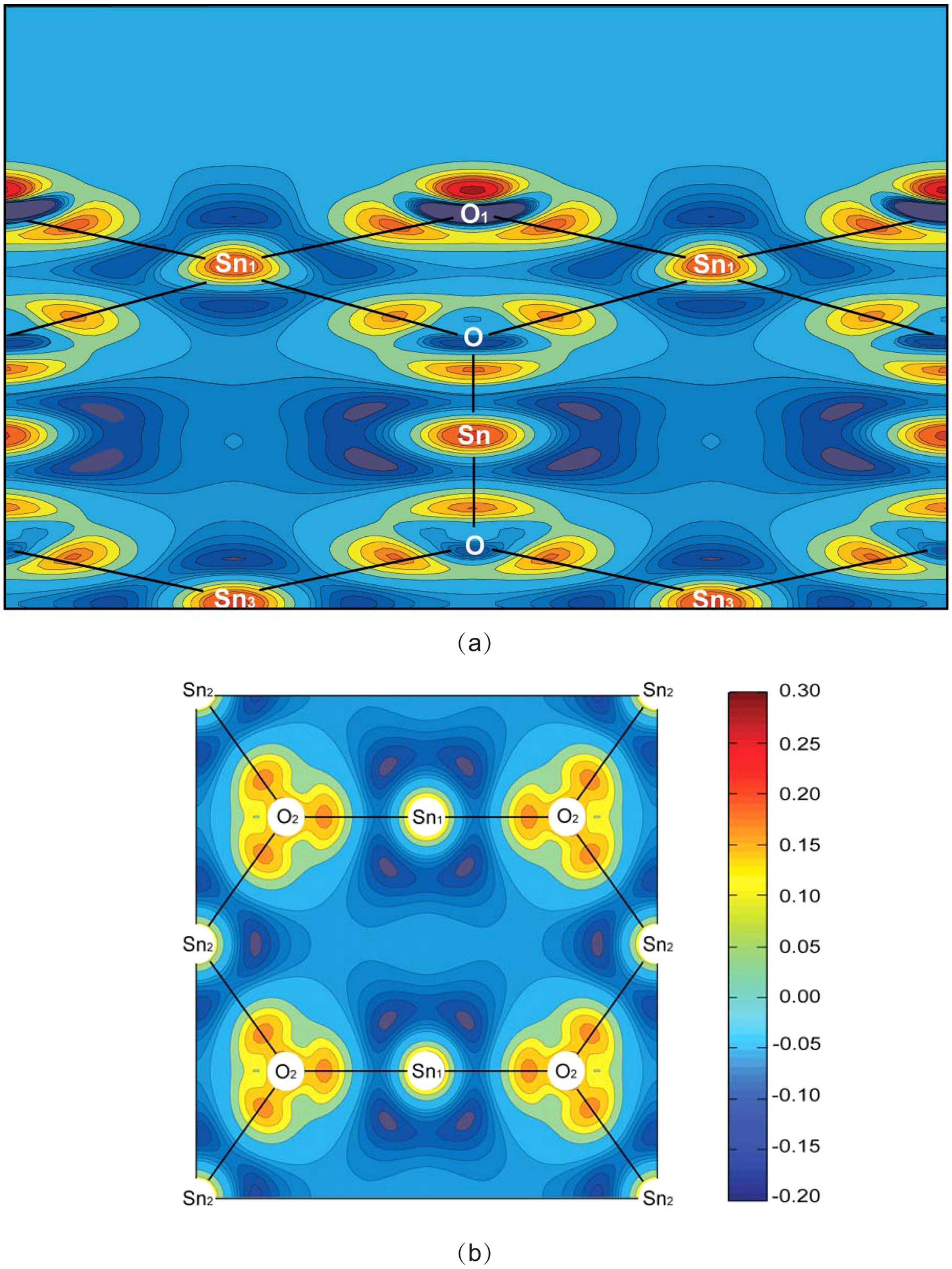

FIG. 7. (Color online) Differential valence charge densities in the units of electrons/Å^3 (a) in the (1–10) plane containing Sn1, O1, and Sn3 and (b) in the (110) plane containing Sn1 and O2.

environment condition, and hence, its stabilized region is absent in Fig. 5.

There unfortunately lacks a direct experimental comparison with our prediction on SnO_2 surface stabilities (versus T and Po_2) shown in Figs. 4 and 5, but our calculations can *well* interpret and clarify one recent experimental observation (see Ref. 41): at T = 1200 K, the highly reduced (101) and (100), i.e., (101)_Sn and (100)_Sn in our Fig. 4, preferentially form at lower oxygen partial pressure; once one increases oxygen partial pressure with keeping temperature unchanged, the growth of (101)_Sn and (100)_Sn ceases automatically and the SnO2 (110) starts to grow preferentially and steadily. Although the authors in Ref. 41 did not provide the exact values of the oxygen partial pressures, the so-called "controlled growth of branched hierarchical crystals with tunable morphology" in Ref. 41 can be regarded as a successful technical application of our theoretically constructed surface stability diagram (i.e., Fig. 4).

It is noticed that all our modeling and simulations were based on one presumption that neglecting vibrational entropy will not change the relative order of surface stability. Direct calculation of vibration entropies of all the surfaces under consideration from the first principles would be computationally over-expensive, due to such large cell sizes and the lack of symmetry. This presumption may introduce some degree of uncertainty to our predicted data values (especially for higher temperatures), but is nevertheless reasonable and found consistent with many experimental observations.[5,10,41,42] Especially in Ref. 41, it has been clearly shown that the SnO_2 (110), the most stable one as we predicted, can be still the most favored surface at even T = 1200 K (and appropriate oxygen partial pressures).

C. Surface electronic structure of SnO_2 (110)

As mentioned above, the stoichiometric (110) is the most stable surface over a large range of environmental conditions. The atomic structures of the (110) stoichiometric surface were presented in Fig. 6(a). The outermost atomic layer is composed of two-coordinated oxygen anions (marked as O_1), which occupy bridging positions between each two six-coordinated Sn cations (Sn_1) located in the second layer. The second atomic layer also includes unsaturated, five-coordinated Sn atoms (Sn_2) as well as fully three-coordinated oxygen atoms (O_2). All Sn and O atoms in the deeper layers of the surface slab are fully coordinated, as in the bulk, and labeled as Sn_3 and O_3 in Fig. 6(a). Atom-projected electronic density of states (DOS) of the stoichiometric (110) is presented in Fig. 6(b). The Fermi energy level denoted by a dashed line is set to zero. It is seen that the occupied states of surface atoms shift up significantly toward the Fermi energy level. Consistent with previous theoretical studies,[10] some clearly localized surface states were observed at the upper valence band region, which caused a reduction of about 1.0 eV in the bandgap. The surface states are quite strongly localized around the bridging oxygens (O1), with some weight on sub-bridging oxygens (O2). As indicated in Fig. 6(b), the surface states are contributed mainly by the hybridization of O1-2p and Sn1-4d orbitals and partially by the hybridization of five-coordinated Sn2-4d and in-plane oxygen O2-2p orbitals. Both theoretical and experimental evidence have indicated that the bridging oxygen atoms are the most active sites on the SnO_2 surface.[5] Compared with those fully coordinated Sn atoms (both Sn_1 and Sn_3), very different conduction structure was observed for the unsaturated, five-coordinated tin atom (Sn2) on the surface, as resulted from the enhanced hybridization of Sn2-5s and O2-2p states. The conduction band minimum is dominated by Sn2-5s character, as also noticed by other calculations,[43] which contributes partially to the reduction of the bandgap. This dispersed s band also contributes to the lowering of optical absorption due to inter-conduction band transitions, which makes SnO_2 a good transparent conductor.[5]

Figure 7 plots the calculated differential valence charge density distribution in the SnO_2 (110) surface region. The charge density difference was computed by subtracting the total charge density of the fully relaxed surface slab from the superposition of isolated atomic charge densities. The charge transfers from tin cations to oxygen anions are obvious in Fig. 7(a), and the accumulated charges around each oxygen anion align along all the three O-Sn bond directions. Due to the presence of surface termination (termination of the periodic potential), the hybridization of Sn-4d and O-2p states is enhanced between Sn1 and O1 compared to that of Sn1 with any other oxygen underneath (labeled as O in Fig. 7(a)). Comparing Fig. 7(a) and Fig. 7(b), one further observes more charge transfer from Sn1 to O1 than to O2. Correspondingly, the bond length of Sn1-O1 has been shortened by 3.8% after surface relaxation, while the length of Sn1-O2 and Sn1-O elongated by 2.4% and 4.8%, respectively.

IV. CONCLUSIONS

The surface stabilities of low-index SnO_2 (110), (101), (100), and (001) surfaces have been studied by density functional theory (DFT) within pseudopotential plane-wave methods. Using a thermodynamic defect model, the surface stabilities were evaluated as functions of oxygen partial pressure and temperature. Both stoichiometric and nonstoichiometric surface with ideal bulk terminations have been considered. The relative ordering of stoichiometric surface stabilities after full relaxation was found to be $(110) > (100) > (101) > (001)$. The stoichiometric to Sn-terminated surface transitions can take place only at ultrahigh vacuum and high temperatures, whereas transitions to the O-terminated were found impossible at any practical environment conditions. The stoichiometric to Sn-terminated transitions always move to higher pressures with increasing temperature. Based on these calculations, an equilibrium surface phase diagram was proposed to illustrate the environment dependence of SnO_2 surfaces. Moreover, the electronic structure of the most stable, stoichiometric SnO_2 (110) surface was investigated by evaluating the electron density of states and differential charge distributions. Clearly localized surface states with a reduced bandgap were observed. The surface states are mainly constituted by the hybridization of bridging oxygen atom O1-2p and six-coordinated tin atom Sn1-4d orbital with partially five-coordinated tin atom Sn2-4d orbital and in-plane oxygen atom O2-2p orbital hybridization.

ACKNOWLEDGMENTS

This paper is based upon work supported by the National Science and Technology support program under Grant No. 2006BAE03B03. The computational resources at High Performance Computing Center of Central South University are also gratefully acknowledged.

[1] B. Thangaraju, Thin Solid Films **402**, 71 (2002).
[2] R. G. Gordon, Mater. Res. Soc. Symp. Proc. **426**, 419 (1996).
[3] R. G. Gordon, J. Proscia, F. B. Ellis, and A. E. Delahoy, Sol. Energy Mater. **18**, 263 (1989).
[4] G. G. Lee and S. J. L. Kang, Sens. Actuators B **107**, 392 (2005).
[5] M. Batzill and U. Diebold, Prog. Surf. Sci. **79**, 47 (2005).
[6] Y. C. Chen, J. M. Chen, Y. H. Huang, Y. R. Lee, and H. C. Shih, Surf. Coat. Technol. **202**, 1313 (2007).
[7] A. Beltrán, J. Andrés, E. Longo, and E. R. Leite, Appl. Phys. Lett. **83**, 635 (2003).
[8] J. Oviedo and M. J. Gillan. Surf. Sci. **463**, 93 (2000).
[9] U. Pulkkinen, T. T. Rantala, T. S. Rantala, and V. Lantto, J. Mol. Catal. A: Chem. **166**, 15 (2001).
[10] M. Batzill, K. Katsiev, J. M. Burst, U. Diebold, A. M. Chaka, and B. Delley, Phys. Rev. B **72**, 165414 (2005).
[11] P. Ágoston and K. Albe, Surf. Sci. **605**, 714 (2011).
[12] See http://cms.mpi.univie.ac.at/vasp for information about the VASP guide.
[13] G. Kresse and J. Joubert, Phys. Rev. B **59**, 1758 (1999).
[14] H. J. Monkhorst and J. D. Pack, Phys. Rev. B **13**, 5188 (1976).
[15] J. P. Perdew, J. A. Chevary, S. H. Vosko, K. A. Jackson, M. R. Pederson, D. J. Singh, and C. Fiolhais, Phys. Rev. B **46**, 6671 (1992).
[16] J. P. Perdew, K. Burke, and M. Ernzerhof, Phys. Rev. Lett. **77**, 3865 (1996).
[17] T. T. Rantala, T. S. Rantala, and V. Lantto, Surf. Sci. **420**, 103 (1999).
[18] F. D. Murnaghan, Proc. Natl. Acad. Sci. U.S.A. **30**, 244 (1944).
[19] J. Oviedo and M. J. Gillan, Surf. Sci. **467**, 35 (2000).
[20] F. R. Sensato, R. Custodio, M. Calatayud, A. Beltrán, J. Andrés, J. R. Sambrano, and E. Longo, Surf. Sci. **511**, 408 (2002).
[21] T. X. T. Sayle, S. C. Parker, and C. R. A. Catlow, Surf. Sci. **316**, 329 (1994).
[22] M. Meyer, G. Onida, M. Palummo, and L. Reining. Phys. Rev. B **64**, 045119 (2001).
[23] V. Golovanov, M. Viitala, T. Kortelainen, O. Cramariuc, and T. T. Rantala, Surf. Sci. **604**, 1784 (2010).
[24] A. A. Bolzan, C. Fong, B. J. Kennedy, and C. J. Howard, Acta Crystallogr., Sect. B: Struct. Sci. **53**, 373 (1997).
[25] A. V. Postnikov, P. Entel, and P. Ordejón, Phase Transitions **75**, 143 (2002).
[26] Y. Jiang, J. B. Adams, and M. V. Schilfgaarde, J. Chem. Phys. **123**, 064701 (2005).
[27] Y. Jiang, J. B. Adams, M. van Schilfgaarde, R. Sharma, P. Crozier, Appl. Phys. Lett. **87**, 141917 (2005).
[28] H. Xu, D. Lee, J. He, S. B. Sinnott, V. Gopalan, V. Dierolf, and S. R. Phillpot, Phys. Rev. B **78**, 174103 (2008).
[29] H. Xu, A. Chernatynskiy, D. Lee, S. B. Sinnott, V. Gopalan, V. Dierolf, and S. R. Phillpot, Phys. Rev. B **82**, 184109 (2010).
[30] K. Reuter and M. Scheffer, Phys. Rev. B **68**, 045407 (2003).
[31] S. Saukkoa, U. Lassib, V. Lanttoa, M. Kroneldc, S. Novikovc, P. Kuivalainenc, T. T. Rantalad, and J. Mizsei, Thin Solid Films **490**, 48 (2005).
[32] Y. Nagasawa, T. Choso, T. Karasud, S. Shimomura, F. Ouyang, K. Tabata, and Y. Yamaguchi, Surf. Sci. **433–435**, 226 (1999).
[33] W. Bergermayera and I. Tanaka, Appl. Phys. Lett. **84**, 909 (2004).
[34] I. Manassidis, J. Goniakowski, L. N. Kantorovich, and M. J. Gillan, Surf. Sci. **339**, 258 (1995).
[35] J. Oviedo and M. J. Gillan, Surf. Sci. **513**, 26 (2002).
[36] A. Bouzoubaa, A. Markovits, M. Calatayud, and C. Minot, Surf. Sci. **583**, 107 (2005).
[37] D. R. Stull and H. Prophet, *JANAF Thermochemical Tables*, 2nd ed. (U.S. National Bureau of Standards, Washington, DC, 1971).
[38] J. Goniakowski, J. M. Holender, L. N. Kantorovich, M. J. Gillan, and J. A. White, Phys. Rev. B **53**, 957 (1996).
[39] B. Slater, C. R. Catlow, D. H. Gay, D. E. Williams, and V. Dusastre, J. Phys. Chem. B **103**, 10644 (1999).
[40] J. E. Dominguez, L. Fu, and X. Q. Pan, Appl. Phys. Lett. **79**, 614 (2001).
[41] J. Liu, X. Chen, W. Wang, B. Song, and Q. Huang, Cryst. Growth Des. **9**, 1757 (2009).
[42] P. Tiirkes, C. Pluntket, and R. Helbig, J. Phys. C **13**, 4941 (1980).
[43] M. A. Mäki-Jaskari, T. T. Rantala, and V. V. Golovanov, Surf. Sci. **577**, 127 (2005).